ChemComm

COMMUNICATION

View Article Online
View Journal | View Issue

Cite this: *Chem. Commun.*, 2025, **61**, 6506

Received 15th January 2025,
Accepted 26th March 2025

DOI: 10.1039/d5cc00250h

rsc.li/chemcomm

An intramolecular phosphine-oxide stabilized germanium(IV) di-cation with enhanced Lewis acidity and catalytic applications†

Akanksha Kumari,[a] Balakrishna Peddi,[a] Cem. B. Yildiz *[b] and Moumita Majumdar *[a]

This work reports the intramolecular phosphine-oxide stabilized tetra-coordinated germanium(IV) di-cation on an acenaphthene platform, 1^{iPr}PO. Computational study shows that the positive charges and the acceptor orbitals are localized on the Ge site. 1^{iPr}PO is Lewis super acidic, capable of catalysing hydrodefluorination reaction. 1^{iPr}PO also catalyses hydrosilylation of electron-deficient aldehydes.

Germanium compounds are less popular as Lewis acids compared to those of silicon[1] analogues due to their inherent higher electronegativity. Contemporary research has shown an upsurge in developing Ge-based Lewis acid catalysts[2] because of their relatively higher stability and thus handling ease. Prominent examples are the bis(perchlorocatecholato) germane and its derivatives[3,4] exhibiting Lewis superacidity and high catalytic aptitude. Geometric constraint was introduced for Lewis acidity enhancement as observed in the anti-van't Hoff-Le Bel reactivity of the calix[4]pyrrolato-germane.[5] Significant increment in the Lewis acidity was noticed by installing positive charges on the Ge centre in the corrole-stabilized planar Ge(IV) mono-cation.[6] The key factor behind the unusually high electrophilicity is the localization of the cationic charge on the Ge centre. There are a few more examples of germylium ions being used as Lewis acid catalysts.[7–9]

Very recently, our group has established the first example of a tetra-coordinated Ge(IV) di-cation as a Lewis acid catalyst (Fig. 1A).[10] The catalytic proficiency of this intramolecular phosphine-stabilized Ge(IV) di-cation was compromised due to the dispersion of the di-positive charges. Therefore, we attempted to localize the acceptor orbitals on the Ge centre of the di-cationic system. A recent study has shown that phosphine oxide serves as an efficient donor towards the cationic sites without significantly hampering their electrophilicity (Fig. 1B and C).[11–14] Inspired by these reports, in our continued efforts for the further advancement of Ge(IV) di-cationic Lewis acids, we have prepared the intramolecular phosphine oxide stabilized Ge(IV) di-cationic compound $\mathbf{1^{iPr}PO}$ (Fig. 1D), exhibiting an expanded catalytic portfolio. The detail is reported herein.

The intramolecular phosphine-oxide stabilized Ge(IV) di-cationic compound on an acenaphthene platform, $\mathbf{1^{iPr}PO}$, was prepared by the simple oxidation of our previously reported compound $\mathbf{1^{iPr}}$,[10] with two equivalents of iodosobenzene in dichloromethane (Scheme 1). Colourless single crystals of $\mathbf{1^{iPr}PO}$ were grown from dichloromethane/pentane layering under room temperature conditions in 75% crystallization yield. Compound $\mathbf{1^{iPr}PO}$ was characterized in the solution state by multi-nuclear NMR spectroscopy in CD_3CN (Fig. S1–S4, ESI†). The $^{31}P\{^1H\}$ NMR chemical shifts at +97.2 ppm (in CD_3CN) and +97.6 (in CD_2Cl_2) were assigned to the phosphorus(V) centre present in $\mathbf{1^{iPr}PO}$. The similar $^{31}P\{^1H\}$ NMR chemical shift values obtained invalidate the

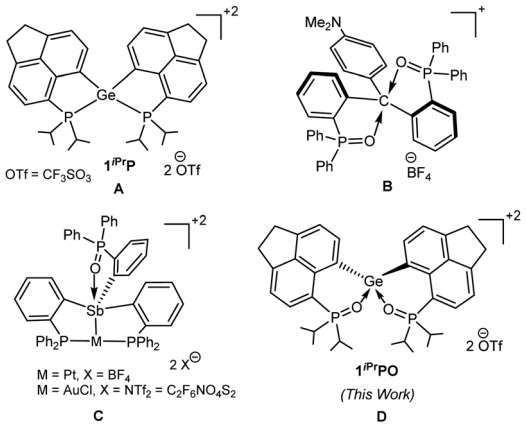

Fig. 1 (A) $\mathbf{1^{iPr}P}$; (B) phosphine-oxide stabilized triaryl carbenium ion; (C) phosphine-oxide stabilized Sb(V) di-cation; and (D) $\mathbf{1^{iPr}PO}$ (this work).

[a] *Department of Chemistry, Indian Institute of Science Education and Research, Pune, Dr Homi Bhabha Road, Pashan, Pune-411008, India. E-mail: moumitam@iiserpune.ac.in*

[b] *Department of Basic Sciences, Faculty of Engineering, Architecture and Design, Bartin University, 74100 Bartin, Turkey*

† Electronic supplementary information (ESI) available. CCDC 2416600, 2416604, 2416606 and 2416610. For ESI and crystallographic data in CIF or other electronic format see DOI: https://doi.org/10.1039/d5cc00250h

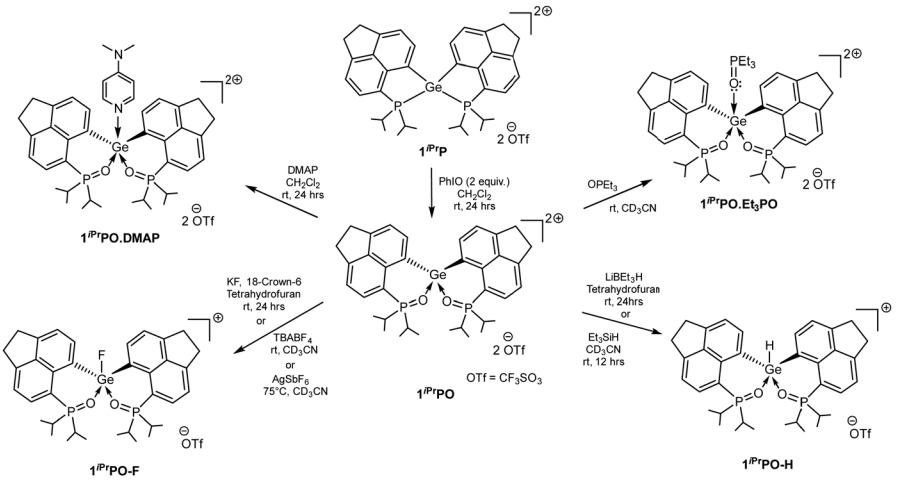

Scheme 1 Lewis base binding and hydride and fluoride ion abstraction (see the ESI,† for detailed spectroscopic and experimental procedures of each reaction).

possible coordination of solvents at the Ge centre.[10] The solid-state structure of **1^{iPr}PO** (Fig. 2 and Table S4, ESI†) shows a spirocyclic geometry with the Ge atom being shared between the two rings. The two triflate (CF_3SO_3 = OTf) counter anions are non-coordinating in nature (closest Ge–O(OTf) contact being 4.3 Å).[15] The average Ge–C bond length in **1^{iPr}PO** (avg. 1.89 Å) is shorter than that observed in the case of **1^{iPr}** (avg. 1.92 Å).[10] The average Ge–O bond length of 1.80 Å lies in the longer range of Ge–O covalent bonds for tetracoordinated Ge(IV) compounds.[16] Correspondingly, the average P–O bond lengths (1.57 Å) exhibit partial double bond character.

The optimized geometry of **1^{iPr}PO** is in close agreement with the X-ray parameters (see ESI,† for the computational detail). The natural bond orbital (NBO) analyses of the optimized structure reveal donor–acceptor interactions between the lone pair orbitals on the oxygen atoms (from phosphine oxide) to the Ge-centred acceptor orbitals (Table S1, ESI†). The NBO frontier molecular orbitals depicted in Fig. 3A show that the acceptor orbitals are localized on the Ge centre, unlike our previously reported **1^{iPr}P** where the acceptor orbitals comprised Ge–C and Ge–P σ* orbitals.[10] The Wiberg bond order (WBO) calculated for Ge–C (0.79) confirms the single bond between them, while the WBO for Ge–O (0.46) echoes the presence of comparatively weaker bonding interaction between them. The low value of WBO for P–O (0.81) reflects less than double bond character. The electrostatic potential map as shown in Fig. 3B reflects the concentration of the positive charges on the Ge centre in **1^{iPr}PO**, as opposed to the dispersed di-positive charges over the P–Ge–P framework found in **1^{iPr}P**. Overall, compared to our earlier report on **1^{iPr}**, our newly synthesized compound **1^{iPr}PO** has di-cationic charges and orbital vacancies localized[6,17] on the Ge-centre.

The effective Lewis acidity[18] of **1^{iPr}PO** following the Gutmann–Beckett (GB) method was investigated (see ESI,† for details). A $\Delta\delta$ ^{31}P value of 25.4 ppm was obtained from the addition of 0.2 equivalents of Et_3PO to **1^{iPr}PO** in CD_3CN (δ for free Et_3PO in CD_3CN is +49.7 ppm; for comparison $\Delta\delta$ ^{31}P for **1^{iPr}P** = 21.3 ppm) (Fig. S7–S9, ESI†). The formation of the mono-adduct **1^{iPr}PO·Et$_3$PO** was confirmed from the ^{31}P NMR study (δ^{iPr}PO at +75.57 ppm and δEt_3PO at +75.08 ppm) (Fig. S10–S12, ESI†). The mono-adduct **1^{iPr}PO·Et$_3$PO** remained in equilibrium with **1^{iPr}PO**, as revealed from the detailed NMR study (Fig. S12, ESI†).

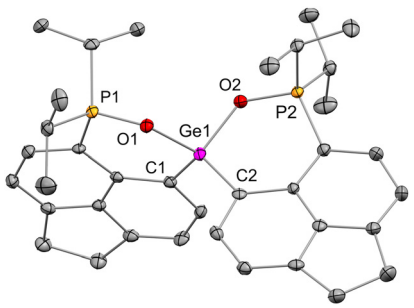

Fig. 2 Molecular structure of **1^{iPr}PO** in the solid state (thermal ellipsoid 35%, H atoms, triflate counter anions and solvent molecules are omitted for clarity). Selected bond lengths [Å] Ge1–O1 = 1.803(2), Ge1–C1 = 1.895(3), P1–O1 = 1.575(2), Ge1–O2 = 1.797(3), Ge1–C2 = 1.891(3), P2–O2 = 1.570(2); selected bond angles [°]: O1–Ge1–C1 = 103.9(1), O2–Ge1–C2 = 104.1(1), O1–Ge1–O2 = 105.1(1), C1–Ge1–C2 = 121.9(1).

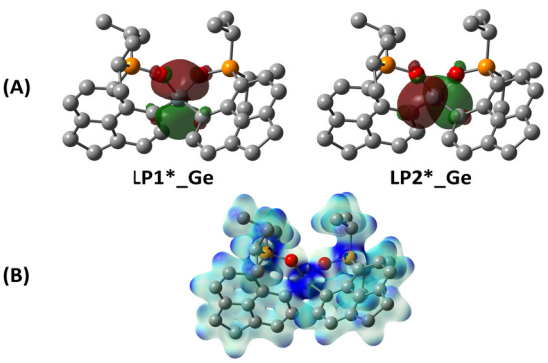

Fig. 3 (A) Natural bond orbitals localized on the Ge center; (B) electrostatic potential map with the range of 0.05 (red)–0.40 (blue).

We were not successful in obtaining single crystals of the adduct **1^{iPr}PO·Et$_3$PO**. Rather, single crystals of the adduct formed with 4-*N*,*N*′-dimethylaminopyridine (DMAP) **1^{iPr}PO·DMAP** (Scheme 1) were obtained. The molecular structure determined showed the coordination of the Lewis base leading to a distorted trigonal bipyramidal geometry at the Ge centre (Fig. S17, ESI†).

We have prepared **1^{iPr}PO-F** from the addition of one equivalent of KF/18-crown-6 to **1^{iPr}PO** (Scheme 1). The $^{31}P\{^1H\}$ NMR in $CDCl_3$ showed a doublet at +77 ppm ($^3J_{P-F}$ = 3.3 Hz) and a corresponding peak at −125.2 ppm in the $^{19}F\{^1H\}$ NMR spectrum (see ESI,† for detail). The molecular structure of **1^{iPr}PO-F** (Fig. 4A and Table S6, ESI†) exhibits a distorted trigonal bipyramidal geometry, analogous to **1^{iPr}PO·DMAP**. The Ge–F bond length is 1.746(2) Å, which is shorter compared to that found in the case of **1^{iPr}P-F** (1.785(2) Å).[10] The Ge–O bond lengths have increased (avg. Ge–O = 1.97 Å) compared to those in **1^{iPr}PO**, with a corresponding decrease in the P–O bond lengths (avg. P–O = 1.53 Å). The calculated gas-phase fluoride ion affinity (FIA)[19] at the Ge site of **1^{iPr}PO** gave a very high value of 865 kJ mol^{-1} (gas-phase FIA for reference SbF_5 is 497 kJ mol^{-1}) (Tables S2 and S3, see the ESI,† details). Incorporation of the acetonitrile (MeCN) solvated model decreased the calculated FIA value significantly to 142 kJ mol^{-1} (solvent corrected FIA for reference SbF_5 is 315 kJ mol^{-1}), respectively. This phenomenon of solvent damping is more pronounced with the cationic Lewis acids compared to the neutral ones.[20,21] Nonetheless, **1^{iPr}PO** was found to be capable of abstracting a fluoride ion from $AgSbF_6$ under heating conditions forming **1^{iPr}PO-F** (Scheme 1). **1^{iPr}PO** also abstracted fluoride from $TBABF_4$ (TBA = *n*-tetrabutylammonium), which is a better fluoride ion donor, to give **1^{iPr}PO-F** under room temperature conditions. Thus, **1^{iPr}PO** proved to be Lewis superacidic[22,23] under experimental conditions, despite low calculated values of FIA in solvated models.[24]

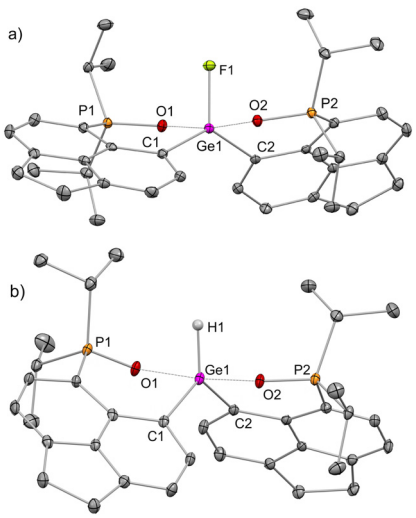

Fig. 4 Molecular structures of (A) **1^{iPr}PO-F** and (B) **1^{iPr}PO-H** in the solid state (thermal ellipsoids 35%, H atoms, triflate counter anions and solvent molecules are omitted for clarity). Selected bond lengths [Å] (a) Ge1–F1 = 1.746(2), Ge1–O1 = 1.971(2), P1–O1 = 1.524(2), Ge1–O2 = 1.990(2), P2–O2 = 1.525(2); (b) Ge1–H1 = 1.436(2), Ge1–O1 = 2.013(2), P1–O1 = 1.520(2), Ge1–O2 = 2.056(2), P2–O2 = 1.517(2).

Gas-phase hydride ion affinity (HIA)[19] calculation (Tables S2 and S3, see ESI† for detail) gave a very high value of 925 kJ mol^{-1}, while incorporation of the solvated model gave low calculated values of 185 KJ mol^{-1} (MeCN). Notably, the gas phase HIA for reference $B(C_6F_5)_3$ is 517 kJ mol^{-1} and the solvent corrected HIA is 244 kJ mol^{-1} for MeCN. Reaction of **1^{iPr}PO** with $NaBH_4$ led to the formation of **1^{iPr}PO-H** (Scheme 1). The $^{31}P\{^1H\}$ NMR spectrum of **1^{iPr}PO-H** displayed a peak at +73.5 ppm. The molecular structure of **1^{iPr}PO-H** closely resembles that of **1^{iPr}PO-F**, possessing a Ge–H bond length of 1.436(2) Å (Fig. 4B and Table S7, ESI†). The inherently hydridophilic Ge center in **1^{iPr}PO** activated the Et_3Si–H bond under room temperature reaction conditions to give **1^{iPr}PO-H** (Scheme 1).[25,26] However, **1^{iPr}PO** does not abstract hydride from Ph_3Si–H[27] even upon heating.

Given the experimentally observed Lewis super acidic nature of **1^{iPr}PO**, we have explored the catalytic hydrodefluorination[28] of an aliphatic C–F bond. With a catalyst loading of 5 mol% **1^{iPr}PO** and employing Ph_3SiH as the hydride source, we have successfully achieved the hydrodefluorination of 1-adamantyl fluoride (76% conversion) in CD_3CN upon heating overnight at 75 °C (Scheme 2A) (see ESI,† for detail). The *in situ* catalytic reaction mixture showed NMR signals at $\delta^{31}P\{^1H\}$ = +77.8 ppm and $\delta^{19}F\{^1H\}$ = −125.8 ppm corresponding to the formation of **1^{iPr}PO-F**, indicating the C–F bond activation over the Si–H bond activation (Fig. S40–S45, ESI†). Thus, we have proposed a catalytic pathway (Scheme S1, ESI†) involving the generation of the carbocation, which then abstracts hydride from Ph_3SiH to form the alkane along with the regeneration of the catalyst **1^{iPr}PO** and Ph_3SiF. We do not observe any Ge–H bond formation as an intermediate, discarding the Ph_3Si–H bond activation pathway by **1^{iPr}PO**. This proposed mechanism is in line with that proposed by Müller *et al.* using the naphthalene-based digermyl hydronium borates as a catalyst.[7] On the other hand, using Et_3SiH as the hydride source for the same catalytic hydrodefluorination reaction (Scheme 2A) turned out to be less promising owing to the competing Si–H bond activation along with C–F bond activation by **1^{iPr}PO**. Only 40% conversion to the corresponding alkane was possible, the catalyst being transformed into **1^{iPr}PO-H** after 12 hours (Fig. S48–S51, ESI†). Notably, catalytic hydrodefluorination was unachievable using **1^{iPr}P** as the catalyst. As a matter of fact, there are very few

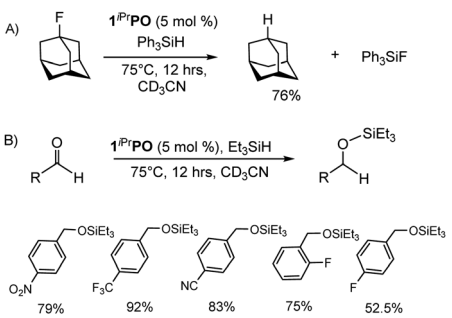

Scheme 2 Catalytic applications of **1^{iPr}PO**: (A) hydrodefluorination of 1-adamantyl fluoride and (B) hydrosilylation of electron-deficient aromatic aldehydes.

reports on catalytic hydrodefluorination reactions achieved using molecular germanium as a catalyst.[3,7,8,17] Our catalyst was ineffective for other C–F bonds. This lack of reactivity may be attributed to the stabilization of the Ge(IV) by the intramolecular P═O donors, thereby compromising the Lewis acidity at the Ge(IV) site.

The hydridophilicity of **1^{iPr}PO** prompted us to explore the substrate scope for the catalytic hydrosilylation reactions (Scheme 2B) of aromatic aldehydes (see ESI,† for detail). In our earlier report, we have shown the catalytic hydrosilylation of *p*-methyl benzaldehyde using **1^{iPr}P** as a catalyst. However, catalytic hydrosilylation of electron-deficient aromatic aldehydes was not possible using **1^{iPr}P**. In this study, we were successful in converting a variety of electron-deficient aldehydes into the corresponding silyl ethers using 5 mol% of **1^{iPr}PO** under mild heating conditions (Scheme 2B).[29]

It was observed from the NMR study that the aldehydes did not bind to the Ge-centre of the catalyst. The NMR investigations of the catalytic reaction mixture showed the formation of a Ge–H bond ($\delta^{31}P\{^1H\}$ = +73.5 ppm) from Et_3Si–H bond activation, corresponding to the formation of **1^{iPr}PO-H** as an intermediate (Fig. S53, see ESI,† for the NMRs). Therefore, the reaction is likely to proceed by Et_3SiH bond activation by **1^{iPr}PO** followed by Si–H addition across the C═O bond in the carbonyls (Scheme S2, see ESI†). A similar mechanism was observed in the case of **1^{iPr}P** as a catalyst. The $^{29}Si\{^1H\}$ NMR spectrum showed the formation of the hydrosilylated products (Fig. S59, ESI†). The formation of Et_3SiOTf as a competent catalyst, though not detected in the NMR spectrum, cannot be completely overruled. The irreversible transformation of the catalyst to **1^{iPr}PO-H** was observed from *in situ* NMR study of the catalytic reaction mixture, which might be responsible for poor catalytic outcome in certain substrates (see ESI,† for detail).

In conclusion, we have successfully manipulated the frontier orbitals by treating **1^{iPr}P** with an oxidant to form the phosphine-oxide stabilized Ge(IV) di-cation **1^{iPr}PO**. Localization of the positive charges and acceptor orbitals on the Ge-centre has significantly enhanced the Lewis acidity. The well-exposed cationic Ge(IV) site is now capable of abstracting fluoride ions from a hexafluoroantimonate anion, thereby marking its Lewis super acidic nature. The hard and soft Lewis acidic nature of **1^{iPr}PO** have been manifested in catalytic hydrodefluorination of 1-adamantyl fluoride and hydrosilylation of electron-deficient aromatic aldehydes, which were unachievable with our previously reported **1^{iPr}P**. Thus, the localization of the cation charges on the Ge-centre has led to the expansion of the catalytic portfolio. Our group is engaged in investigating further catalytic applications of **1^{iPr}PO**, and extending this catalyst design strategy to other main-group Lewis acids.

M. M. thanks SERB India SPF/2022/000046 and CRG/2022/000673 for financial support. A. K. thanks UGC for the fellowship. We thank Prof. Deepak Chopra from the Indian Institute of Science Education and Research (IISER) Bhopal, India for his help in crystallography.

Data availability

Experimental details, spectroscopic data, X-ray diffraction analysis data, and computational data are available in the ESI.†

Conflicts of interest

There is no conflict to declare.

Notes and references

1 H. Yamamoto and M. Oishi, *Silicon(IV) Lewis Acids*, Wiley-VCH, Weinheim Germany, 2000.
2 N. Mukherjee and M. Majumdar, *J. Am. Chem. Soc.*, 2024, **146**, 24209.
3 D. Roth, H. Wadepohl and L. Greb, *Angew. Chem., Int. Ed.*, 2020, **59**, 20930.
4 A. T. Henry, T. P. L. Cosby, P. D. Boyle and K. M. Baines, *Dalton Trans.*, 2021, **50**, 15906.
5 R. Yadav, P. Janβen, M. Schorpp and L. Greb, *J. Am. Chem. Soc.*, 2023, **145**, 177546.
6 H. Fang, H. Jing, A. Zhang, H. Ge, Z. Yao, P. J. Brothers and X. Fu, *J. Am. Chem. Soc.*, 2016, **138**, 7705.
7 N. Kordts, C. Borner, R. Panisch, W. Saak and T. Müller, *Organometallics*, 2014, **33**, 1492.
8 A. Hayatifar, A. Borrego, D. Bosek, M. Czarnecki, G. Derocher, A. Kuplicki, E. Lytle, J. Padilla, C. Paroly, G. Tubay, J. Vyletel and C. S. Weinert, *Chem. Commun.*, 2019, **55**, 10852.
9 M. Talavera, G. Meiβner, S. G. Rachor and T. Braun, *Chem. Commun.*, 2020, **56**, 4452.
10 B. Peddi, S. Khan, R. G. Gonnade, C. B. Yildiz and M. Majumdar, *Chem. Sci.*, 2023, **14**, 13755.
11 (*a*) J. E. Smith, H. Yang and F. P. Gabbaï, *Organometallics*, 2021, **40**, 3886; (*b*) Y.-H. Lo and F. P. Gabbaï, *Angew. Chem., Int. Ed.*, 2019, **58**, 10194.
12 E. D. Litle and F. P. Gabbai, *Chem. Commun.*, 2024, **60**, 690.
13 M. Olaru, R. Kather, E. Hupf, E. Lork, S. Mebs and J. Beckmann, *Angew. Chem., Int. Ed.*, 2018, **57**, 5917.
14 W.-C. Liu and F. P. Gabbaï, *Science*, 2024, **385**, 1184.
15 A. Bondi, *J. Phys. Chem.*, 1964, **68**, 441.
16 S. E. Denmark, R. T. Jacobs, G. Dai-Ho and S. Wilson, *Organometallics*, 1990, **9**, 3015.
17 D. Tanaka, A. Konishi and M. Yasuda, *Chem. – Asian J.*, 2021, **16**, 3118.
18 P. Erdmann and L. Greb, *Angew. Chem., Int. Ed.*, 2022, **61**, e202114550.
19 P. Erdmann, J. Leitner, J. Schwarz and L. Greb, *Chem. Phys. Chem.*, 2020, **21**, 987.
20 A. Hermannsdorfer and M. Driess, *Angew. Chem., Int. Ed.*, 2020, **59**, 23132.
21 D. Roth, J. Stirn, D. W. Stephan and L. Greb, *J. Am. Chem. Soc.*, 2021, **143**, 15845.
22 L. O. Müller, D. Himmel, J. Stauffer, G. Steinfeld, J. Slattery, G. SantisoQuiñones, V. Brecht and I. Krossing, *Angew. Chem., Int. Ed.*, 2008, **47**, 7659.
23 T. Thorwart and L. Greb, Lewis Superacids, in *Encyclopedia of Inorganic and Bioinorganic Chemistry*, ed. R. A. Scott, Wiley, 2nd edn, 2021, pp. 1–26.
24 P. Erdmann, M. Schmitt, L. M. Sigmund, F. Krämer, F. Breher and L. Greb, *Angew. Chem., Int. Ed.*, 2024, **63**, e202403356.
25 G. I. Nikonov, S. F. Vyboishchikov and O. G. Shirobokov, *J. Am. Chem. Soc.*, 2012, **134**, 5488.
26 A. Y. Houghton, J. Hurmalainen, A. Mansikkamaki, W. E. Piers and H. M. Tuononen, *Nat. Chem.*, 2014, **6**, 983.
27 Z. M. Heiden and A. P. Lathem, *Organometallics*, 2015, **34**, 1818.
28 G. Meier and T. Braun, *Angew. Chem., Int. Ed.*, 2009, **48**, 1546.
29 A. L. L. Martin, R. G. Bergman and T. D. Tilley, *J. Am. Chem. Soc.*, 2015, **137**, 5328.